Computationally Efficient Transient Stability Modeling of multi-terminal VSC-HVDC

Arjen. A. van der Meer, José Rueda-Torres, Filipe Faria da Silva, M. Gibescu, Mart A. A. M. van der Meijden, *Members, IEEE*

***Abstract*--This paper studies the inclusion of averaged VSC-based grid interfaces and HVDC networks into stability type simulations, and compares the accuracy and speed of three multi-terminal DC dynamic models: 1) a state-space based model, 2) a multi-rate improved model, and 3) a reduced-order model. The accuracy comparison is conducted by qualitative time-domain analysis taking the state-space model as a reference whereas the computational aspects are investigated by the respective execution times. The models are demonstrated on a three VSC terminal, two synchronous area system. It is shown that the reduced-order model is too inaccurate to investigate detailed large-disturbance stability-related dynamics. The multi-rate model shows the best trade-off between simulation accuracy and speed.**

***Index Terms*--Transient Stability Simulation, VSC-HVDC, Multi-Rate Techniques.**

I. Introduction

RECENT developments in power electronics have led to the large-scale deployment of voltage sourced converters (VSC) for high power applications. On transmission level, the application of high-voltage DC (HVDC) transmission based on modular multi-level converter (MMC) VSC is becoming mainstream technology [1]. This offers interesting new options for future network expansions, such as integrating large amounts of offshore wind power and the establishment of transnational offshore grids based on DC technology [2].

Future networks must be analyzed in detail in planning studies performed today. An important part of such studies are transient stability simulations. The incorporation of power electronic interfaces, particularly VSCs, into them is a major challenge [3]. VSC dynamics are several orders of magnitude faster than machine dynamics. In themselves these fast dynamics are not very important for transient stability, which would justify the use of reduced-order VSC models. Unfortunately, electrical transients induced by power electronics might trigger control features or protective circuits that may have a significant influence on AC system dynamics.

Most transient stability analysis tools do not offer a structural solution to this problem, and each type of power electronics device requires careful individual consideration, especially when extending beyond point-to-point links to multi-terminal DC (MTDC), present methods are insufficient.

This paper studies the inclusion of VSC-based grid interfaces and arbitrary DC networks into stability type simulations, and compares the accuracy and numerical performance of the following HVDC models:

- a state-space model using a π-sectional branch representation [4, 5]
- a multi-rate implementation of this model; and
- a reduced-order (copper-plate) model, similar to [6].

We determine the accuracy qualitatively by comparing the time domain results after test disturbances, taking the state-space model as a reference. This paper introduces an innovative model that employs multi-rate techniques [7]. This method uses smaller time steps for numerical integration, allowing parts of the system that require more detail to be solved separately from the main solution algorithm. This permits arbitrary DC structures to be simulated with high accuracy and minor speed impairment, while no additional (external) EMT simulation is involved. For this research a new stability-type simulation framework is developed to experiment with several numerical solution methods, model-to-network interfaces, and dynamic model implementations.

The paper starts with a description of this simulation framework. Subsequently, the VSC model is discussed, emphasizing on its protection and control mechanisms. We continue with describing the various DC grid dynamic models and their inclusion into the simulation routine. Next, the models' applicability for transient stability studies and their numerical performance (i.e. simulation speed) will be demonstrated using an example system. The paper ends with conclusions.

II. Simulation Framework

Stability-type simulations have been developed to investigate the electromechanical interactions in AC power systems [8]. Advancements in numerical methods and computational power over the past decades have made it possible to study large AC power systems for a wide variety of disturbances and phenomena. These simulations model the power system as a set of non-linear differential-algebraic equations (DAE) as

$$\dot{\mathbf{x}} = \boldsymbol{f}(\mathbf{x}, \mathbf{y}) \tag{1}$$

$$\mathbf{0} = \boldsymbol{g}(\mathbf{x}, \mathbf{y}) \tag{2}$$

where $\mathbf{x}$ and $\mathbf{y}$ are the set of state variables and algebraic variables respectively. $\boldsymbol{f}$ is the differential function and

This research is executed in cooperation with TenneT TSO B.V and Energinet.dk under the COBRAcable project and co-financed by the European Commission under the European Energy Program for Recovery. It is a joint project of Delft University of Technology and Aalborg University

A. A. van der Meer is with Delft University of Technology, Mekelweg 4, 2628 CD, the Netherlands (e-mail: a.a.vandermeer@tudelft.nl).

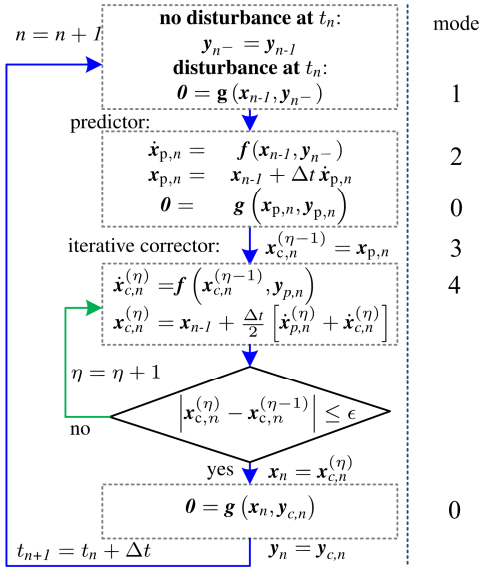

Fig. 1. Predictor-corrector calculation sequence for one stability simulation time step n. Subscripts p and c represent the predictor and corrector vectors respectively. η is the corrector iteration counter.

commonly describes the machine, the governor, and the excitation system dynamic behavior. $\boldsymbol{g}$ is the algebraic function and contains the network equations, the models' current injections, and the behavior of static loads.

We use the solution scheme of Fig. 1, showing the calculation sequence for a typical fixed time step at t_n. The simulation uses *Heun's method*, employing a forward-Euler predictor and an iterative trapezoidal corrector.

Dynamic models are called using the modes shown right of each calculation step. The algorithm distinguishes between a predictor call (mode=2) and the first corrector call (mode=3) and subsequent corrector calls (mode=4). $\boldsymbol{f}$ is called at least twice per time-step, depending on the corrector tolerance $\boldsymbol{\varepsilon}$.

Unless a disturbance occurs at t_n (mode=1), $\boldsymbol{g}$ is solved after the predictor step and the last corrector step (mode=0). This solution follows a Newton-Raphson iterative scheme, which first calculates the mismatch by

$$\boldsymbol{g}^{(\zeta)} = \boldsymbol{r}\left(\mathbf{x}, \mathbf{y}^{(\zeta-1)}\right) - \mathbf{y}^{(\zeta-1)} \tag{3}$$

in which $\boldsymbol{r}$ estimates $\mathbf{y}$ based on $\mathbf{y}^{(\zeta-1)}$ at the ζ^{th} algebraic iteration. $\mathbf{y}^{(\zeta)}$ is then calculated by

$$\mathbf{y}^{(\zeta)} = \mathbf{y}^{(\zeta-1)} - \mathbf{J}^{-1}\boldsymbol{g}^{(\zeta)} \tag{4}$$

where $\mathbf{J} = \partial\mathbf{g}/\partial\mathbf{y}$ is the Jacobian matrix containing the sensitivities of each algebraic function to its particular variables. $\mathbf{J}$ is determined by the forward difference method [9], which is computationally complex. Therefore, the very dishonest method is used here, keeping $\mathbf{J}$ fixed unless mode=1, or after an iteration threshold for ζ. Eq. (3) and (4) are repeated until convergence.

The simulation framework is in-house developed (using Python) and is motivated by the desire to experiment with several numerical solutions for (1) and (2), a feature that commercial tools essentially do not offer. This versatile tool offers the modeling and solution flexibility that is indispensable for a sound comparison between the VSC-HVDC models discussed next.

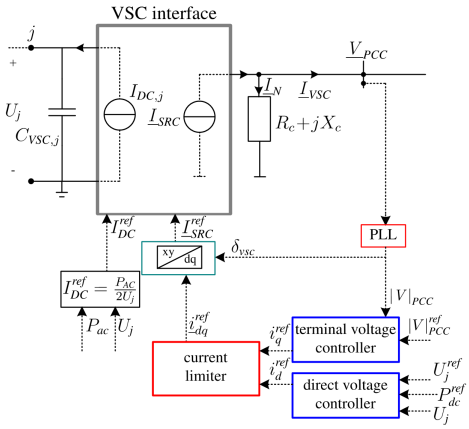

Fig. 2. VSC dynamic model for transient stability simulations.

III. VSC Modeling

The dynamic VSC-MTDC model implemented for this paper consists of 1) a *VSC model* which provides the interaction between the VSC controls and the AC network, 2) A *power balance model* which regulates the AC/DC interaction and the fault-ride through (FRT) behavior, and 3) an *MTDC model* modelling the HVDC transmission and hence the coupling between VSC models.

A. VSC Model

We use the averaged VSC model as shown in Fig. 2 [10]. It represents the DC side by a variable current source, and the AC side by a time varying Norton complex current injection.

1) Control Scheme

VSCs connected to relatively strong AC systems commonly use vector control, which allows independent control of active and reactive power. By using a PLL-controlled *dq*–reference frame, its terminal voltage is controlled in such a way that the VSC behaves as a current source. The Norton current injection is given by

$$\underline{I}_{\text{SRC}} = \frac{\underline{V}_{\text{PCC}}}{R_c + \text{j}X_c} + \underline{i}_{\text{VSC, dq}}^{\text{ref}} \text{e}^{\text{j}\delta_{\text{PLL}}} \tag{5}$$

in which $\underline{i}_{\text{VSC, dq}}^{\text{ref}} = i_{\text{d}}^{\text{ref}} + \text{j}i_{\text{q}}^{\text{ref}}$ are set by the direct voltage and the terminal voltage controllers. For the AC/DC interaction, the former is more significant and controls $i_{\text{d}}^{\text{ref}}$ as follows:

$$i_{\text{d}}^{\text{ref}} = \frac{P_{\text{PCC}}^{\text{ref}}}{|V|_{\text{PCC}}} = \frac{e_{\text{d}}}{|V|_{\text{PCC}}}\left(k_{\text{d}} + \frac{1}{\tau_{\text{d}}}\int \text{d}t\right) + i_{\text{d,0}} \tag{6}$$

where e_{d} is the control error between the DC power (i.e. P_j) and its reference value according to a droop characteristic

$$e_{\text{d}} = P_{\text{dc},j}^{\text{ref}} + \left(U_j^{\text{ref}} - U_j\right)\frac{1}{D} - P_j \tag{7}$$

where D is the droop constant in the VSC's per unit system. The bandwidth of the PI-controller in (6) should be high to adequately react to fast direct voltage variations.

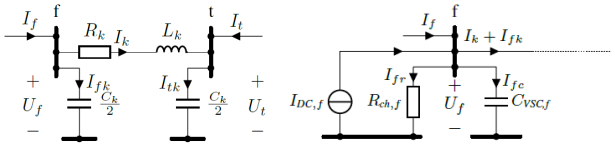

Fig. 3. Branch models for cables (left) and VSC shunts (right).

2) DC-side Representation

To stay connected during AC faults, VSCs are equipped with chopper-controlled braking resistors, which is assumed to trigger at a 1.1 pu threshold value of U_j. This can be modelled either by variable resistors $R_{\mathrm{ch},f}$ or by variations in the active power delivered to the DC side.

Because of the symmetrical nature of the AC network model, this paper assumes an equal distribution of power among both poles of the DC side of the VSC. Hence, a monopolar representation of the DC scheme is used to save computational power. At the DC side, the VSC exhibits current source behavior due to the control scheme and the connected phase reactors. Therefore, the AC/DC interaction of the VSC is governed by the active power balance as

$$I_{\mathrm{dc},j} = \frac{P_j}{2U_j} = -\frac{(P_\mathrm{c} - P_\mathrm{loss} - P_\mathrm{ch})}{2U_j} \tag{8}$$

where P_c is the VSC terminal power, P_loss are the switching losses, and P_ch is the power absorbed by the braking resistor.

IV. MTDC REPRESENTATION

A. State-Space Representation of MTDC Transmission

Since stability simulations are particularly designed to study AC systems, HVDC transmission should be incorporated by user-written dynamic models. This is achieved by developing a general state-space representation of the HVDC transmission. It uses the DC nodal current injections (i.e. $I_{\mathrm{dc},j}$) of the VSC power balance models as inputs, and provides the DC nodal voltages (i.e.U_j) as input quantities for the VSC models.

Fig. 3 shows the branch models being used. Submarine cables are modelled by their π-equivalent, whereas the VSCs' DC-side capacitors and braking resistors are modelled by an RC shunt branch.

Assuming the general case of having a VSC, and hence shunt branches, at both sides of the submarine cable, the electro-magnetic interactions can be described by

$$\frac{\mathrm{d}U_f}{\mathrm{d}t} = \frac{1}{C_{\mathrm{VSC},f} + \frac{C_k}{2}} \left(I_f + I_{\mathrm{dc},f} - I_k - \frac{U_f}{R_{\mathrm{ch},f}} \right) \tag{9}$$

$$\frac{\mathrm{d}U_t}{\mathrm{d}t} = \frac{1}{C_{\mathrm{VSC},t} + \frac{C_k}{2}} \left(I_t + I_{\mathrm{DC},t} + I_k - \frac{U_t}{R_{\mathrm{ch},t}} \right) \tag{10}$$

$$\frac{\mathrm{d}I_k}{\mathrm{d}t} = \frac{1}{L_k} \left(U_f - U_t - I_k R_k \right) \tag{11}$$

where U_f and U_t are the *from* and *to* node voltages respectively, I_k the branch current, I_{dc} the nodal current injections provided by (8), I_f and I_t the sum of the branch currents connected to f and t, and R_{ch} the braking resistors. This system of three first-order differential equations can be cast into state-space formulation, with I_{dc} as system inputs.

This concept is generalized to arbitrary topologies by treating the MTDC grid as a directed graph using the current direction as a reference, and subsequently determining the adjacency matrix with

$$M_{\mathrm{a},kj} = \begin{cases} 1 & \text{if branch } k \text{ connects from node } j \\ -1 & \text{if branch } k \text{ connects to node } i \\ 0 & \text{otherwise} \end{cases} \tag{12}$$

where $\mathbf{M}_\mathrm{a}$ is the $K \times J$ unreduced adjacency matrix, with K and J the total amount of branches and nodes respectively. Shunt branches always connect *to* the ground, which is taken as the reference node. The column corresponding to the reference node is removed from $\mathbf{M}_\mathrm{a}$ to obtain the adjacency matrix $\mathbf{M}$, which contains no linearly dependent columns. Using $\mathbf{M}$, the system of equations of an arbitrarily structured MTDC scheme can be generalized as

$$\begin{aligned} \dot{\mathbf{x}}_{\mathrm{dc}} &= \boldsymbol{f}_{\mathrm{dc}}(\mathbf{x}_{\mathrm{dc}}, \mathbf{y}_{\mathrm{dc}}) = \mathbf{A}\mathbf{x}_{\mathrm{dc}} + \mathbf{B}\mathbf{y}_{\mathrm{dc}} \\ &= \left[\begin{array}{c|c} -\mathbf{R}_{\mathrm{ch}}\mathbf{C}_{\mathrm{aux}} & -\mathbf{C}_{\mathrm{aux}}\mathbf{M}^T \\ \hline \mathbf{L}_{\mathrm{aux}}\mathbf{M} & -\mathbf{R}_{\mathrm{aux}}\mathbf{L}_{\mathrm{aux}} \end{array}\right] \left[\begin{array}{c} \mathbf{u}_{\mathrm{dc}} \\ \hline \mathbf{i}_{br} \end{array}\right] \\ &+ \left[\begin{array}{c|c} \mathbf{C}_{aux} & \mathbf{0}_{J\times K} \\ \hline \mathbf{0}_{K\times J} & \mathbf{0}_{K\times K} \end{array}\right] \left[\begin{array}{c} \mathbf{i}_{\mathrm{dc}} \\ \hline \mathbf{0}_{K\times 1} \end{array}\right] \end{aligned} \tag{13}$$

where $\mathbf{x}_{\mathrm{dc}}$ and $\mathbf{y}_{\mathrm{dc}}$ are the state and algebraic input vectors, $\mathbf{A}$ and $\mathbf{B}$ the state and input matrices, $\mathbf{u}_{\mathrm{dc}}$ the vector with DC node voltages, $\mathbf{i}_{\mathrm{br}}$ the shunt and cable currents, and $\mathbf{i}_{\mathrm{dc}}$ the input nodal current injections. The model contains no pure voltage sources, a plausible assumption for VSC-HVDC.

$\mathbf{R}_{\mathrm{ch}}$ is the $K \times K$ diagonal matrix containing the chopper-resistors in case these are modelled by variable resistances instead of variations in the active power balance. Its elements are given by

$$R_{\mathrm{ch},kk} = \begin{cases} \frac{1}{R_{\mathrm{ch},k}} & \text{if } R_{\mathrm{ch},k} \neq 0 \text{ and } k \leq K_{\mathrm{sh}} \\ 0 & \text{otherwise} \end{cases} \tag{14}$$

The first K_{sh} branches are assumed shunt branches. $\mathbf{C}_{\mathrm{aux}}$ is an $J \times J$diagonal matrix defined by

$$C_{\mathrm{aux},j,j} = \begin{cases} \frac{1}{C_{\mathrm{bus,j}}} & \text{if } C_{\mathrm{bus,j}} \neq 0 \\ 0 & \text{otherwise} \end{cases} \tag{15}$$

where

$$C_{\mathrm{bus},j} = \sum_{k=1}^{K_{\mathrm{sh}}} C_k M_{kj} + \sum_{k=K_{\mathrm{sh}}+1}^{K} \frac{C_k}{2} \left| M_{kj} \right| \tag{16}$$

$\mathbf{L}_{\mathrm{aux}}$ is a $K \times K$ diagonal matrix containing the cable inductances as

$$L_{\mathrm{aux},kk} = \begin{cases} \frac{1}{L_k} & \text{if } L_k \neq 0 \\ 0 & \text{otherwise} \end{cases} \tag{17}$$

and $\mathbf{R}_{\mathrm{aux}} = \mathrm{diag}\left[R_1\ R_2 \ldots R_K\right]$ the $K \times K$ diagonal matrix containing the cable resistances.

B. Multi-rate Improvement

The state-space model requires Δt~0.1 ms, leading to prohibitive execution times. This is resolved by separating the solution of (1) of both the MTDC system and the VSCs' FRT controls from the slower dynamic models, and by simulating these models at a smaller Δt_{mr}. This multi-rate technique is applied by use of the inner integration loop shown in Fig. 4. It starts with a forward-Euler integration step of the MTDC model. Then the obtained DC state variables are used to invoke the FRT model, which determines the DC nodal current

injections for the next time step of the inner integration loop. At step m, the DC current injection at node j is given by

$$I^m_{\mathrm{dc},j} = \frac{P^m_j}{2U^m_j} = -\frac{\left(P_c|_{m=0} - P_{\mathrm{loss}}|_{m=0} - P^m_{\mathrm{ch}}\right)}{2U^m_j} \tag{18}$$

which makes the current injection dependent on both AC side power available at $m = 0$ and the power calculated by the FRT model. The implementation proposed here does not require $\mathbf{A}$ and $\mathbf{B}$ to be rebuilt every time step. Hence, it makes sense to model the FRT controls as power variations in (18) rather than variable network elements in $\mathbf{A}$. Including the FRT model into the inner integration loop improved the numerical stability of the simulation, thereby allowing a higher Δt.

At the end of the inner integration loop, the vectors of the main solution algorithm must be updated to be compliant with both the predictor and the trapezoidal corrector. This is done by calculating the slope based on the first $(x^{m-\frac{\Delta t}{\Delta t_{\mathrm{mr}}}})$, and the last calculated state, i.e. x^m.

In case numerous corrector iterations are necessary, it is too time-consuming to execute the inner-integration loop continually. Therefore, we assume the numerical integration routine accurate enough to be invoked only during the first corrector step (i.e. mode=3).

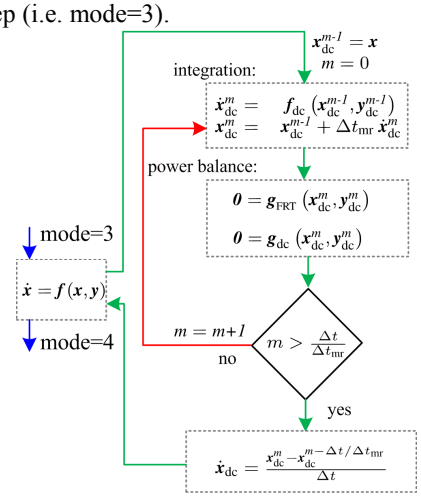

Fig. 4. VSC dynamic model for transient stability simulations.

C. Reduced-order State-Space MTDC Model

Another option to allow a larger Δt is to simplify the state space model to a one-node equivalent DC hub, similar to what has been proposed in [6]. This copper-plate assumption lumps all the pole-to-ground capacitance of the DC cables and the VSC shunts, and neglects all DC-side inductive elements. The DC dynamics are then given by

$$\frac{\mathrm{d}U_{\mathrm{dc}}}{\mathrm{d}t} = \frac{1}{C_{\mathrm{dc}}}\left(\sum_{j=1}^{J} I_{\mathrm{dc},j} - \frac{P_{\mathrm{loss},0}}{U_{\mathrm{dc}}}\right) \tag{19}$$

where U_{dc} is the direct voltage, $C_{\mathrm{dc}} = \sum_{j=1}^{J} C_{\mathrm{bus},j}$, $I_{\mathrm{dc},j}$ is the nodal current injections vector for all J DC nodes, and $P_{\mathrm{loss},0}$ are the total HVDC cable losses calculated at t_0 from the power flow initialisation step. U_{dc} is initialized at the average of all DC nodal voltages at t_0.

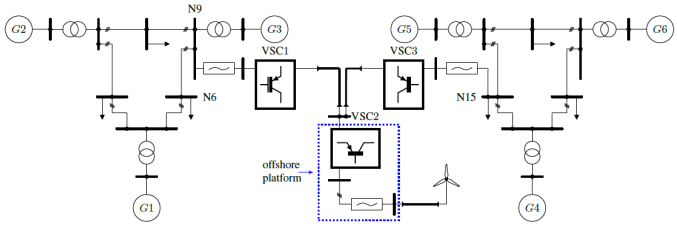

Fig. 5. Test system used for comparing VSC-HVDC dynamic models.

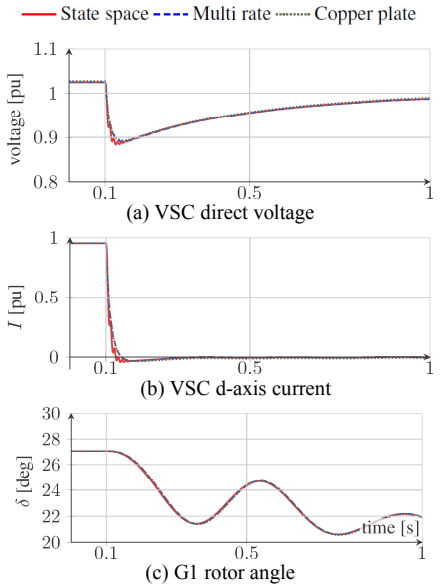

Fig. 6. Response after a 600 MW load rejection by VSC3

V. Simulation Studies

A. Simulation Setup

The 3 MTDC models discussed in this work will be tested for accuracy (taking the state space model validated in [11] as a reference) and computational performance (i.e. executing times). The test system is shown in Fig. 5. It contains 2 identical IEEE 9-bus systems, which are linked by a 3-terminal VSC-HVDC scheme that integrates a type 4, 600 MW offshore wind park. All generators have standard TGOV1 governing and SEXS excitation systems. VSC1 and 3 are in vector control mode, using continuous AC voltage magnitude control and DC voltage droop regulation. In case the VSCs' current limits are hit, the current references are limited proportionally across $i^{\mathrm{ref}}_{\mathrm{VSC},d}$ and $i^{\mathrm{ref}}_{\mathrm{VSC},q}$

B. Response to a Load Rejection by VSC2

First, the system will be subjected to a load rejection by VSC2 (which is a rejection of generation as seen from the system's side). Fig. 6 shows the system response and compares the three discussed MTDC dynamic models.

The power imbalance caused by VSC2 causes the direct voltage to drop quickly. The droop controllers of VSC1 and VSC3 react to this by practically stopping their active power output. The generators in both AC systems have to re-establish their own power balance. Despite the severity of this disturbance its influence on the response of the individual MTDC models is not clearly perceptible; all models suffice.

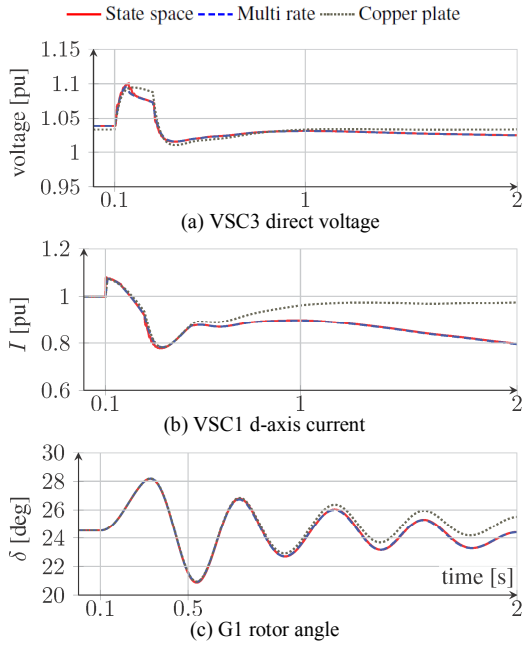

(a) VSC3 direct voltage

(b) VSC1 d-axis current

(c) G1 rotor angle

Fig. 7. System response after a 180 ms bus fault at N6

TABLE I: SIMULATION TIME STEP-SIZE AND EXECUTION TIMES

model	Δt(ms)	Δt_{mr}(ms)	Fig. 6 (s)	Fig. 7 (s)
state space	1	n/a	50	500
multi-rate	10	0.1	17.6	111
reduced-order	10	n/a	10.7	82

C. Response to a Short Circuit at N6

Next, we simulate a 180 ms fault at N6. The output of the offshore wind park is 180MW while VSC3 injects 130MW into the DC scheme. The system on the left (Fig. 5) imports power. Fig. 7 compares the MTDC models. The differences between the model dynamics are now more prominent, especially for $i_{C,d}$ of VSC1 and δ of G1. The discrepancy between the reduced-order model and the reference simulation is caused by the fact that just one direct voltage is available to the VSC models. For the reduced-order model, the FRT system of VSC3 does hence not trigger on the elevated direct voltage, as is the case with the other MTDC dynamic models. This inaccuracy is a direct consequence of the model reduction– as the FRT models use the local direct voltage.

D. Computational Performance

Table I shows the execution times of all simulations, which have been performed on a Windows 7 workstation (i7-2630QM CPU, 4 GB RAM). The execution times are much higher compared to (commercial) compiled software because the environment was implemented by Python scripting

We can observe that the short-circuit case took considerably longer compared to the load rejection case. This difference can be attributed to the higher amount of re-determinations of the Jacobian matrix. Nevertheless the differences between the MTDC models are plainly observable. Due to the small time constants in the DC system, the state-space model had to be simulated using a smaller Δt for the entire network, thereby strongly reducing the efficacy of the stability-type simulation. Both suggested MTDC modelling improvements could be simulated at a higher Δt and are hence faster.

VI. CONCLUSIONS

Modelling VSC-HVDC transmission inside stability-type simulations is challenging because of the trade-off that must be made between simulation speed and modelling accuracy. This is mainly caused by the small time constants that are present in the MTDC system. To answer the question as to whether the effect of these time constants on the AC system dynamics could be ignored, this paper described and tested 3 dynamic models for transient stability simulations applicable for systems containing multi-terminal VSC-HVDC transmission. These are: 1) a state space model using a π-equivalent representation of the DC grid, 2) a multi-rate enhancement, and 3) a reduced-order model which models the DC grid by an aggregated capacitance The paper focused on generalizing the modelling approach for multi-terminal purposes as well as the inclusion of the MTDC grid model into the solution algorithm of the stability-type simulation.

Simulations illustrated the dynamic behavior of the proposed models. For small-signal disturbances the reduced-order model showed favorable execution speed and a plausible response. For short circuits, this model was less accurate, which can be attributed to the copper-plate assumption made. This inhibits massive application for transient stability assessment. The multi-rate model gives a good trade-off between the desired accuracy and execution speed.

VII. REFERENCES

[1] C. Oates, "Modular multilevel converter design for vsc hvdc applications," *IEEE Journal of Emerging and Selected Topics in Power Electronics*, vol. 3, no. 2, pp. 505–515, Jun. 2015.

[2] J. Dragon, L. F. Beites, M. Callavik, D. Eichhoff, J. Hanson, A.-K. Marten, A. Morales, A. Sanz, F. Schettler, D. Westermann, S. Wietzel, R. Whitehouse, and M. Zeller, "Development of functional specifications for hvdc grid systems," in *Proc. IET AC and DC Power Transmission Conference*, Birmingam, UK, Feb., "10-12,", 2015.

[3] J. Beerten, O. Gomis-Bellmunt, X. Guillaud, J. Rimez, A. A. van der Meer, and D. van Hertem, "Modelling and control of HVDC grids: a key challenge for the future power system," in *18th Power System Computation Conference*, Wroclaw, Poland, Aug. 18–22 2014.

[4] S. Cole, J. Beerten, and R. Belmans, "Generalized dynamic vsc mtdc model for power system stability studies," *IEEE Transactions on Power Systems*, vol. 25, no. 3, pp. 1655 –1662, aug. 2010.

[5] P. J. D. Chainho, A. A. van der Meer, R. L. Hendriks, M. Gibescu, and M. A. M. M. van der Meijden, "General modeling of multi-terminal vsc-hvdc systems for transient stability studies," in *Proc. 6th IEEE Young Researchers Symposium in Electrical Power Engineering*, Delft, the Netherlands, Apr. 16–17 2012.

[6] F. Shewarega and I. Erlich, "Simplified modeling of vsc-hvdc in power system stability studies," vol. 19, 2014, pp. 9099–9104.

[7] R. Pandey, "Stability analysis of ac/dc system with multirate discrete-time hvdc converter model," *Power Delivery, IEEE Transactions on*, vol. 23, no. 1, pp. 311–318, Jan 2008.

[8] B. Stott, "Power system dynamic response calculations," *Proceedings of the IEEE*, vol. 67, no. 2, pp. 219–241, Feb. 1979.

[9] U. M. Ascher and L. R. Petzold, Computer Methods for Ordinary Differential Equations and Differential-Algebraic Equations. Siam, 1997.

[10] "Guide for the development of models for hvdc converters in a hvdc grid," Technical Brochure 604 Working Group B4.57, Cigré, Dec. 2014.

[11] A. A. van der Meer, M. Ndreko, M. Gibescu, and M. A. M. M. van der Meijden, "The effect of FRT behavior of VSC-HVDC connected offshore wind power plants on AC/DC system dynamics," vol. PP, no. 99, p. 1, accepted for publication.